

Phase-transition effects in BaTiO₃ from tight-binding energy bands

L. Castet-Mejean and F. M. Michel-Calandini

Laboratoire de Physique Electronique, Université Lyon-1, 43, Boulevard du 11 Novembre 1918,
Villeurbanne-Cedex, 69622, France

(Received 7 July 1980)

The behavior of the complex electronic dielectric constant ϵ in cubic and tetragonal BaTiO₃ crystals has been deduced from tight-binding energy bands, revealing an anisotropy in agreement with experimental data. The single- and two-oscillator parameters obtained from calculated ϵ functions are used in the interpretation of the optical properties and polarization-induced effects. The upper oscillator is found polarization dependent. The phase transition induces a remarkable decrease of interband transition strengths along the polar axis and an upward shift of transition energies. The ionic charges, deduced from band results through a population analysis, allow one to estimate the spontaneous polarization in the tetragonal phase. The electro-optic effects are investigated from calculated birefringency, polarization, and oscillator parameters. Optical and electro-optic properties are due to transitions in a relatively wide spectral region.

I. INTRODUCTION

Semi-empirical tight-binding computations of the optical properties of cubic ABO_3 perovskites have recently shown the influence of tight-binding parameters on the complex electronic dielectric constant $\epsilon(E)$ versus photon energy,¹ this strong dependence being clearly revealed on the spectra when the interband transition momentum matrix elements $P_{ij}(\vec{k})$ are evaluated for each \vec{k} wave vector in the Brillouin zone. This first work allowed us to set up new band computations for BaTiO₃ and KNbO₃ which provided a rather reliable x-ray photoelectronic spectra (XPS) description of these crystals.² Further investigations of the optical properties of cubic and tetragonal KNbO₃ crystals³ have been handled with the parameter set reported in Ref. 2 allowing an estimation of the spontaneous polarization and some electro-optic parameters in the tetragonal phase.

The purpose of the present work is to complete these studies to provide an interpretation of the optical properties and of the polarization-induced anisotropy by performing similar computations for cubic and tetragonal BaTiO₃. The tetragonal phase has been investigated using crystallographic data and atomic displacements determined by Harada⁴ at 18°C. The determination of $\epsilon(E)$ functions in cubic and tetragonal phases is reported in Sec. II and an evaluation of two-oscillator Sellmeier model parameters performed on the band structure allows a meaningful discussion about the optical properties. An electronic population analysis provides the theoretical crystal ionic charges in the two phases. This allows us to estimate the spontaneous polarization P_s as described in Sec. III. Some of the electro-optic effects are deduced from the theoretical anisotropy and

polarization. They are compared to existing experimental data.

II. DIELECTRIC CONSTANT AND RELATED OPTICAL PROPERTIES

A. Computational details

The component $\epsilon_\mu = \epsilon_{1\mu} + i\epsilon_{2\mu}$ of the complex dielectric function, for a light polarized in direction $\vec{\mu}$, due to interband transitions, is determined in the self-consistent-field approach⁵ through the expression

$$\epsilon_\mu(E) = 1 - \frac{e^2 \hbar^2}{\epsilon_0 m^2 \Omega} \sum_{\vec{k}} \sum_{i,j} \frac{|P_{ij}^\mu(\vec{k})|^2}{E_{ij}^2} \times \frac{f_0(E_j(\vec{k})) - f_0(E_i(\vec{k}))}{E_{ij} - E - i\hbar/\zeta} \quad (1)$$

with the interband momentum matrix elements $P_{ij}(\vec{k})$ given in the effective-mass approximation⁶ by

$$P_{ij}^\mu(\vec{k}) = \frac{m}{\hbar} \sum_{l,n} C_{i,l}^*(\vec{k}) \frac{\partial H_{l,n}(\vec{k})}{\partial k_\mu} C_{n,j}(\vec{k}), \quad (2)$$

where E_{ij} is the energy difference between the j th and i th \vec{k} states, Ω is the unit-cell volume, $f_0(E)$ is the Fermi function, taken to be zero or one, respectively, for an empty or an occupied band. The relaxation time ζ gives a linewidth to the ij interband transition, and is taken less than 10^{-12} s in order to give no artificial enlargement of ϵ_μ curves. In the $P_{ij}^\mu(\vec{k})$ expression, $C_{il}(\vec{k})$ denotes the expansion coefficient of the l th Bloch atomic orbital in the i th state while $H_{l,m}(\vec{k})$ is the Hamiltonian matrix element between the l and m Bloch orbitals. In the present work, i and j stand, respectively, for O $2p$ and Ti $3d$ bands while

the atomic Bloch orbitals retained in $H_{1,m}(\vec{k})$ estimations present the O 2s, O 2p, and Ti 3d symmetries.

The moments of ϵ_2 , computed according to the expression given by Wemple *et al.*⁷

$$M_n = \frac{2}{\pi} \int_{E_i}^{E_r} E^n \epsilon_2(E) dE \quad (3)$$

are used to estimate the oscillator parameters defined by

$$\begin{aligned} E_0 &= (M_{-1}/M_{-3})^{1/2}, \\ E_d &= (M_{-1}^3/M_{-3})^{1/2}, \\ F &= E_0 E_d, \end{aligned} \quad (4)$$

where F_0 is the oscillator strength, E_d the dispersion energy (considered as an interband strength parameter), and F the oscillator strength in the single-oscillator (SO) and the two-oscillator (TO) models, commonly used in the interpretation of ordinary index measurements and electro-optic parameters. In the SO case, all interband transitions are taken into account and the sum-rule integral extends from $E_i = 0$ eV to $E_r = 15$ eV (considered as a maximum energy for O 2p-Ti 3d interband width). In the TO model, the lower frequency oscillator, usually ascribed to transitions towards the lower conduction-band subgroup, is denoted by index ϵ and the integration can be restricted to $E_r < 6$ eV, while the second oscillator, denoted by γ , describes transitions towards the higher part of the conduction band, the energies E ranging between $E_i \geq 6$ eV and $E_r \leq 15$ eV. The optical functions determined in the tetragonal phase will be identified by a supplementary subscript a (or c) in order to represent a light polarized perpendicular (or parallel) to the spontaneous polarization \vec{P}_s .

B. Dielectric function in the paraelectric phase

The theoretical determination of optical functions from relation (1) implies a careful sampling of the Brillouin zone in order to obtain reliable histograms. Several computations have been performed with an increasing number of equivalent \vec{k} points inside the Brillouin zone (BZ). When no interpolation procedure is applied to obtain energies and wave functions between the \vec{k} points where the secular determinant is solved, 8000 equivalent points appear to be the minimum which ensures stable histograms; this number leads also to the equality of the values of $\epsilon_1(0)$ obtained directly from relation (1) or derived from the ϵ_2 moment $M_{-1} + 1$. To get some insight into the optical properties from energy bands, faster computational procedures commonly used in the literature express the ϵ_2 behavior by the joint density of state $J(E)$, or alternatively by the $J(E)/E^2$ func-

tion. This approximation emphasizes the part played by level positions in the band scheme and misses out totally any selectivity between the strengths of optical transitions. In the case of perovskite compounds, the high value of the dielectric constant is usually ascribed to closely spaced energy levels. The evaluation of $\epsilon(E)$ function through expression (1) reveals the presence of strong oscillator strengths at specific \vec{k} points inside the BZ, related to the band bending at these points, and responsible for the $\epsilon_2(E)$ behavior. Independent of a specific report of $P_{ij}(\vec{k})$ variations versus \vec{k} vectors, devoted to a forthcoming paper, the previous remarks are clearly illustrated by the line shape of $J(E)$, $J(E)/E^2$, and $\epsilon_2(E)$ curves plotted in Fig. 1. The first two functions exhibit two important maxima around 5.2 and 6.4 eV while only one dominant structure, localized between 3.6 and 5 eV, is visible both in theoretical and experimental ϵ_2 spectra, a huge decrease of ϵ_2 intensity is observed in the 5–7-eV region, the oscillator strengths being weak. The $J(E)/E^2$ curve is flattened to high energies due to the factor E^2 , whereas the strong values of $P_{ij}(\vec{k})$ connecting the O 2p states to the higher energy subgroup of the conduction bands restore the ϵ_2 structure above 8 eV. Another positive advantage of an exact determination of ϵ function is that absolute magnitudes of ϵ_1 and ϵ_2 curves are obtained, and the quite good agreement between calculated and experimental $\epsilon_1(0)$ data ensures that oscillator parameters

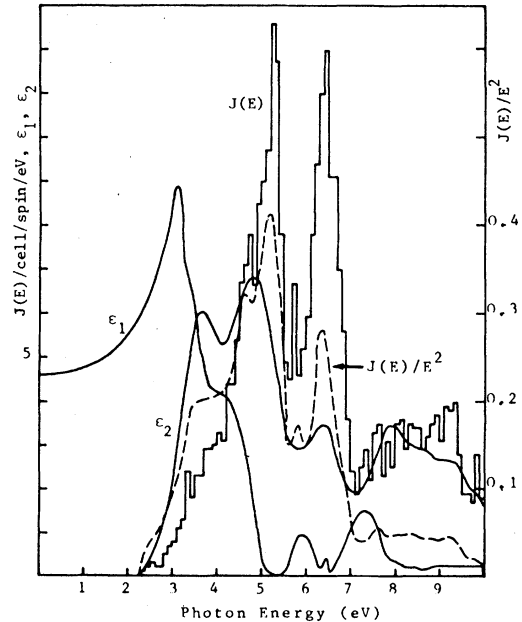


FIG. 1. Real (ϵ_1) and imaginary (ϵ_2) parts of the optical dielectric constant vs photon energy, compared with the joint density of states $J(E)$ and $J(E)/E^2$ function (dashed line) in cubic BaTiO₃.

TABLE I. Single- and two-oscillator parameters and refractive index in BaTiO₃ crystals.

Phase	SO parameters				TO parameters		
	Reference	E_0 (eV)	E_d (eV)	$E_{0\epsilon}$ (eV)	$E_{d\epsilon}$ (eV)	$E_{0\gamma}$ (eV)	$E_{d\gamma}$ (eV)
cubic	a	4.78	16.26	4.12	9.06	7.88	9.30
tetragonal $\vec{\mu} \parallel \vec{a}$	a	4.90	16.06	4.21	8.77	8.08	9.52
	b	5.66	24.00	4.20	6.20	10.50	29
$\vec{\mu} \parallel \vec{c}$	a	5.06	15.69	4.37	8.71	8.14	8.86
	b	5.95	24.22	4.36	5.8	10.50	29
	References	$n_a(1 \text{ eV})$	$n_c(1 \text{ eV})$	$n_a(2 \text{ eV})$	$n_c(2 \text{ eV})$		
	c	2.101	2.057	2.220	2.163		
	d	2.104	2.052	2.230	2.168		
	e	2.132	2.086	2.283	2.217		

^aThis work.^bReference 10.^cEstimated from relation (5) in the SO description.^dEstimated from relation (5) in the TO description.^eDeduced from ϵ_1 values [relation (1)].

can be reliably deduced from energy-band results. The main structure in the ϵ_2 curve presents two peaks localized around 3.7 and 4.9 eV, similar to the experimental data,⁸ the dominating optical transitions are roughly centered around 4.4 eV. This value coincides with the effective oscillator position $E_{0\epsilon} = 4.43$ eV deduced by Johnston⁹ from ordinary index measurements in flux-grown BaTiO₃ at room temperature. The cubic oscillator parameters, evaluated as described in Sec. II A, are gathered in Table I and discussed hereafter.

C. Dielectric constant in the ferroelectric phase

The atomic displacements $\Delta\alpha$ ($\alpha = \text{Ba, Ti, O}_1, \text{O}_2, \text{O}_3$) determined by Harada *et al.*⁴ on BaTiO₃ crystals at 18 °C are used to compute the Madelung energy shifts and the changes in overlap and transfer integrals induced by the cubic to tetragonal phase transition. The changes of the relevant tight-binding parameters, together with the crystal symmetry lowering, are responsible for the anisotropy exhibited by theoretical ϵ_1 and ϵ_2 curves owing to light polarization. These curves are compared in Fig. 2 to Cardona's data, obtained with unpolarized light on samples presenting a random orientation of ferroelectric domains. Considering these measurement conditions, theoretical and experimental spectra appear coherent. The dominating optical transitions, estimated from the first maxima of ϵ_{2c} , ϵ_{2a} spectra are centered around 4.6 eV ($\vec{\mu}$ along \vec{c} axis) and 4.5 eV ($\vec{\mu}$ along \vec{a} axis). These energies qualitatively determined compare well with a more significant computa-

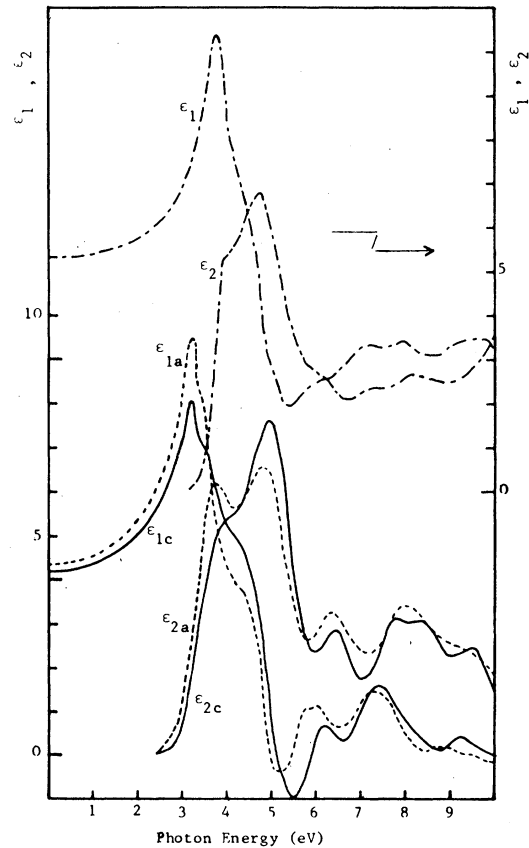


FIG. 2. Light polarization dependence of the dielectric function in tetragonal BaTiO₃: ϵ_{1a} and ϵ_{2a} curves (---), ϵ_{1c} and ϵ_{2c} curves (—), experimental ϵ_1 and ϵ_2 spectra taken from Ref. 8 (---).

tion of the first oscillator positions given by Uchida¹⁰ and also calculated by ourselves: $E_{0\epsilon c} = 4.36$ eV and $E_{0\epsilon a} = 4.2$ eV (Table I). The anisotropy is more apparent for the lower energies because it is more localized: the first peak of ϵ_{2c} at 3.9 eV is strongly smoothed over and the second one at 5 eV is raised. The opposite effect holds for $\vec{\mu}$ perpendicular to the \vec{P}_s axis. This behavior is quite similar to the one of experimental reflectivity spectra reported by Gähwiller.¹¹ In the TO model, Johnston⁹ found one optical transition, or possibly a closely spaced transition group, localized around 5 eV, which is polarization dependent. The ϵ_2 anisotropy allows us to localize these transitions more precisely around 3.8 and 5 eV. The spontaneous polarization involves an enlargement of P_{ij}^c moments around 5 eV and a decrease of them near 3.8 eV.

The TO model reveals the polarization dependence of the γ oscillator as it will be pointed out below. The oscillator parameters, estimated through SO and TO models are gathered in Table I, with the experimental ones deduced by Uchida.¹⁰ The main discrepancy concerns the γ parameters, which are weaker than Uchida's data. This can be easily understood by considering that 4s and higher excited Ti states have been neglected in the present tight-binding computations, dropping out part of the possible high-energy transitions. Moreover, transitions above 15 eV are discarded in the sum-rule integral (3) whereas the experimental ϵ_2 spectrum¹² shows small structures between 15 and 30 eV. The contributions to the γ oscillator are restricted and the effect on $E_{d\gamma}$ is about three times stronger than on $E_{0\gamma}$ due to the fact that ϵ_2 underestimation affects mainly the moment M_{-1} . Nevertheless the observed discrepancies being independent of light polarization and of crystal symmetry, a meaningful interpretation of the phase-transition effects or polarization-induced changes on these parameters may be attempted. On the other hand Uchida and Johnston have assumed that the position and the strength of the γ oscillator are polarization independent, but actually, we find comparable changes of the ϵ and γ parameters caused by the phase transition and owing to light polarization, as it can be deduced from Table I. We can note that, at high energies P_s is reflected in the transition strength ($E_{d\gamma c} - E_{d\gamma a} = -0.66$ eV) rather than in the displacement of the transitions ($E_{0\gamma c} - E_{0\gamma a} = 0.06$ eV) while the opposite effect holds at low energies. The cubic to tetragonal phase transition induces a similar decrease (0.35 and 0.44 eV) of the $E_{d\epsilon}$ and $E_{d\gamma}$ parameters for a light vector along \vec{P}_s . In the perpendicular direction $E_{d\gamma}$ increases by 0.22 eV and $E_{d\epsilon}$ decreases by 0.29 eV. In the tetragonal phase these parameters are weaker along the polar axis than those perpendicular to it. It appears, therefore, that spontaneous polarization saturates part of the optical dielectric constant. The effect of \vec{P}_s parallel to its

axis, from the cubic to the tetragonal phase, besides the remarkable reduction of interband transition strengths, is an upward shift of 250 meV for ϵ and γ E_{0c} oscillators; it would amount to a rigid displacement of transitions, independent of \vec{k} vectors, as it was found by Gähwiller for an $E_{0\epsilon a}$ oscillator under an applied electric field parallel to the c axis. But this is only an average effect, the different \vec{k} states move independently. We can note the interband gap shift to the phase transition at Γ point is 100 meV when the shift between a - and c -axis band edges determined experimentally¹³ is 110 meV. This can be compared with $E_{0c} - E_{0a} \approx 200$ meV found by Wemple¹³ or with our result $E_{0c} - E_{0a} = 150$ meV for the SO positions. A customary approximation consists, in the absence of cubic experimental data, of the tetragonal a axis as a reference in the estimation of phase-transition-induced effects. Results of Table I or ϵ_1 curves below the threshold energy (Figs. 1 and 2) show non-negligible differences between cubic and tetragonal a -axis data, and the phase-transition effects are slightly stronger than the effects due to orientation of $\vec{\mu}$ in the tetragonal phase. The TO model will be now used for the estimation of the respective part played by the ϵ and γ parameters on birefringency and refractive index.

D. Refractive index and birefringency

The frequency dependence of the refractive index n , deduced from ϵ_1 spectra, is plotted in Fig. 3 for the two phases and according to the orientations of light vector $\vec{\mu}$ (i.e., n_a and n_c) and compared to the curves of Wemple *et al.*¹⁴ Johnston's data⁹ as well as Wemple's, are larger than the calculated ones at low energies. This can be justified through relation (5) that expresses n in the region of transparency, since the second oscillator is underestimated, as pointed out just before. But the first oscillator is preponderant as the energy is closer to the threshold and the refractive index spectra rise over the experimental ones, computed ϵ parameters being strong. The respective contribution of each oscillator to the refractive index can be estimated by using the expan-

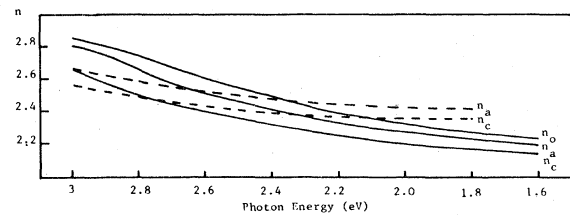


FIG. 3. Dispersion of the refractive indices in cubic (n_0) and tetragonal phase (n_a, n_c): (—) deduced from theoretical ϵ functions and (---) experimental spectra taken from Ref. 14.

sion of $\epsilon_1(E)$ (Ref. 7) in powers of E^2 yielding the relation

$$\epsilon_1 - 1 = n^2 - 1 = \frac{E_{d\epsilon}E_{0\epsilon}}{E_{0\epsilon}^2 - E^2} + \frac{E_{d\gamma}E_{0\gamma}}{E_{0\gamma}^2 - E^2} \quad (5)$$

This approximation involves an error less than 3% for the determination of n and is all the more accurate as the considered frequencies are far from the threshold energy. As an example, we reported in Table I the refractive index values for 1 and 2 eV, deduced from ϵ_1 computations and from relation (5) with the E_d and E_0 parameters determined previously. Single- and two-oscillator representations give a correct estimation of n , but a further insight into the nature of optical anisotropy is provided by the two-oscillator model.

The contribution of ϵ and γ oscillators to the birefringency can be shown to be of the same order, from relation (5). The anisotropies, involving transitions up to 15 eV, have an influence on the birefringency in the visible part of the spectrum as it was already deduced by Wiesendanger and Guntherodt¹⁵ for orthorhombic KNbO₃ considering transitions up to 10 eV. The calculated birefringency at 0.546 μm is $\Delta n = 0.07$, close to experimental data reported earlier by Wemple and Di Domenico,¹⁴ $\Delta n = 0.061$, or by Johnston,⁹ $\Delta n = 0.05$

III. SPONTANEOUS POLARIZATION AND ELECTRO-OPTIC PARAMETERS

The partial densities of states of O $2p$ and Ti $3d$ characters have been estimated from band results in

O_h^1 and C_{4v}^1 symmetries, according to the procedure described in a preceding work.¹⁶ This allows us to obtain the crystal ionic charges on titanium and oxygens by convenient summations over the energies of occupied states. Results relevant to tetragonal case are gathered in Table II. A slight electron transfer from transversal oxygens ($O_2, O_3 \equiv O_{\perp}$) towards the axial one ($O_1 \equiv O_{\parallel}$) is observed; the axial position appears more ionic than the transversal ones, as in KNbO₃,³ but in this latter case, the ionicity changes are due to an electronic exchange between Nb and O₁₁ ions. In a previous work, the electronic structure of cubic BaTiO₃ crystal has been investigated by performing $X\alpha$ self-consistent computations on an octahedral TiO₆⁻⁷ cluster.¹⁷ The population analysis of $X\alpha$ electronic distributions leads to a Ti ionic charge of about 1.9, quite similar to the value obtained from band structure (≈ 2). A decrease of about $2|e|$ in the ionicity on central ion B relatively to the perfectly ionic value has been observed in a lot of ferroelectric ABO_3 compounds (SrTiO₃, KNbO₃, KTaO₃), when population analyses are performed on their electronic structures obtained by various approaches: $X\alpha$ cluster method,¹⁷ augmented plane wave-linear combination of atomic orbitals (APW-LCAO) band schemes¹⁸ or the previous³ and present tight-binding computations. In spite of the ambiguities inherent in a Mulliken population analysis, this steady decrease is not an effect of computational procedure and expresses very probably the correct degree of covalency in such perovskites. Indeed, the calculated charges have their origin in partial densities of states leading to a quite good interpretation of covalency ef-

TABLE II. Ionic and apparent charges, spontaneous polarization, and unclamped electro-optic parameters for BaTiO₃.

References	Charges and spontaneous polarization								P_s (cm ⁻²)
	Q_{Ba}	Q_{Ti}	$Q_{O_{\parallel}}$	$Q_{O_{\perp}}$	Q''_{Ba}	Q''_{Ti}	$Q''_{O_{\parallel}}$	$Q''_{O_{\perp}}$	
a	2.0	1.99	-1.35	-1.32	4.14	4.12	-2.06	-4.13	0.22
b					2.9	6.7	-2.4	-4.8	0.27
c	1.4	2.2	-1.2	-1.2	3.6	5.7	-3.1	-3.1	0.25
d	1.35	2.46	-1.27	-1.27					0.16

References	Polarization-optic coefficients					Polarization potentials		
	g_{11}	g_{12} (m ⁴ /C ²)	$g_{11} - g_{12}$	f_{33} (m ² /C)	f_{13}	β_{11}	β_{12} (eV m ⁴ /C ²)	$\beta_{11} - \beta_{12}$
a	0.39	0.16	0.24	0.17	0.07	5.75	2.60	3.15
e			0.14					3.2
f and g			0.12			6.3	0	

^aThis work.

^bReference 20.

^cReference 21.

^dReference 23.

^eReference 9.

^fReference 14, at $\lambda = 0.633 \mu\text{m}$.

^gReference 13.

fects in photoelectron spectra relevant to these crystals.^{16,17}

To evaluate electro-optic effects we estimate the spontaneous polarization through the relation

$$P_s = \frac{e}{\Omega} \sum_{\alpha} Q_{\alpha}'' \Delta d_{\alpha}$$

by using the concept of apparent charges Q'' introduced by Cochran,¹⁹ as reported in a previous paper.³ For a diagonally cubic crystal the apparent cation charges are

$$Q'' = \frac{1}{3} (\epsilon_{\infty} + 2) Q'$$

where Q' are the effective ionic charges. Axe has found in the local-field approximation²⁰ that this relation is still a good approximation in the tetragonal phase and the ratio Q''/Q' is not far from the Q''/Q for several perovskites. The high-frequency dielectric constant ϵ_{∞} along c axis deduced from relation (1) is 4.203, weaker than the experimental one 5.31 as we expected, owing to the two oscillator model interpretation. The anisotropy of the apparent charges of the two types of oxygens can be taken into account using the ratio $Q''_{O_{\parallel}}/Q''_{O_{\perp}} = 2$ (Ref. 20) obtained from infrared dipole strengths. The absolute values of Q''_{O_i} are deduced from the requirement of the total apparent charge neutrality. These apparent charges, together with the atomic displacements of Ref. 4, lead to the P_s value. These results are compared in Table II to Hewatt's data,²¹ the effective charges being estimated from Cowley's SrTiO₃ results²² and with the choice $Q''_{Ti}/Q''_{Ba} = 1.6$, and to these of Axe's²⁰ with $Q_{Ti}/Q_{Ba} = 2$, and to Bouillot's values computed from the shell model.²³

The main discrepancy may be ascribed to the choice of the Q_{Ti}/Q_{Ba} ratio. The value 1.6 is near the ratio Q_{Ti}/Q_{Ba} chosen by Kahn and Leyendecker²⁴ to compute the Madelung energies and the ionization energies in SrTiO₃ crystals. It is also close to the ratio chosen by ourselves to set up the Hamiltonian diagonal elements since $Q_{Ti} = 2.99|e|$ and $Q_{Ba} = 2|e|$ in the beginning of the computation. The present tight-binding calculations have not been carried out to self-consistency, since it has been found that it is impossible to obtain simultaneously self-consistency upon the charges, and agreement between theoretical and experimental optical functions such as band gap or dielectric constant.² This misleading effect seems inherent in the nature of the approximations involved in the determination of diagonal matrix elements. In the present work, the ratio Q_{Ti}/Q_{Ba} ob-

tained from the population analysis is reduced to about 1; once more, this result is coherent with $X\alpha$ self-consistent results,¹⁷ where the self-consistency upon energies and potentials is achieved, with a simultaneous good reproduction of the main features of BaTiO₃ crystal properties. This coherence between theoretical results obtained by two different computational procedures seems to us a positive point to ensure the reliability of our Q_{Ti}/Q_{Ba} ratio, as well as the relevant calculated P_s value (0.22 C/m²), which agrees fairly well with experiment.²⁵

The unclamped quadratic and linear polarization-optic coefficients g_{11}, g_{12} and f_{33}, f_{13} (reduced notation), are determined for the wavelength $\lambda = 0.6 \mu\text{m}$, from the relation reported by Wemple and Di Domenico²⁵ and are compared to available experimental results in Table II. They are higher than the latter but our P_s value is weaker and some approximations discussed in Sec. II C lead to some disagreements concerning the refractive index. The part played by the ϵ and γ oscillator in the refractive index changes from the cubic to the tetragonal phase in the region of transparency discussed previously, stresses the importance of the high- and low-lying p - d charge transfer transitions for the unclamped electro-optic effect in BaTiO₃. In the polarization potential concept, a single oscillator description is used and the results are compared to average interband polarization potentials calculated by Di Domenico and Wemple.²⁶ The difference $\beta_{11} - \beta_{12} = 3.15 \text{ eV m}^4/\text{C}^2$ is close to Johnston's data⁹: $3.2 \text{ eV m}^4/\text{C}^2$.

IV. CONCLUSION

The theoretical determination of the optical properties involves some approximations that could explain some disagreements observed between calculated and experimental data. However the computation of the moment P_{ij}^{μ} for every \vec{k} vector allows us to carry out the dielectric constant determination, emphasizing the polarization-induced anisotropy. The sum rules applied to the band structure allow us to determine independently the γ and ϵ oscillator parameters. This determination provides an interpretation of the optical properties, setting off the part played by the high-energy transitions for BaTiO₃. The optical anisotropy and the optical property changes induced from the cubic to the tetragonal phase, can be described from Madelung energy shifts, overlap and transfer integral changes, and lowering of crystal symmetry. Their respective influences will be described more extensively in a further paper.

- ¹L. Castet-Mejean and F. M. Michel-Calendini, *J. Phys. C* 11, 2195 (1978).
- ²P. Pertosa and F. M. Michel-Calendini, *Phys. Rev. B* 17, 2011 (1978).
- ³L. Castet-Mejean and F. M. Michel-Calendini, *Ferroelectrics* 25, 475 (1980).
- ⁴J. Harada, T. Pedersen, and Z. Barnea, *Acta Crystallogr. Sect. A* 26, 336 (1970).
- ⁵H. Ehrenreich and H. H. Cohen, *Phys. Rev.* 115, 786 (1959).
- ⁶G. Dresselhauss and M. S. Dresselhauss, *Phys. Rev.* 160, 649 (1967).
- ⁷S. H. Wemple and M. Di Domenico, Jr., *Phys. Rev. B* 3, 1938 (1971).
- ⁸M. Cardona, *Phys. Rev. A* 140, 651 (1965).
- ⁹A. R. Johnston, *J. Appl. Phys.* 42, 3501 (1971).
- ¹⁰N. Uchida, *J. Appl. Phys.* 44, 2072 (1973).
- ¹¹Ch. Gähwiller, *Solid State Commun.* 5, 65 (1967).
- ¹²D. Bauerle, W. Brawn, V. Saile, G. Sprussel, and E. E. Koch, *Z. Phys. B* 29, 197 (1978).
- ¹³S. H. Wemple, *Phys. Rev. B* 2, 2679 (1970).
- ¹⁴S. H. Wemple, M. Di Domenico, Jr., and I. Camlibel, *J. Phys. Chem. Solids* 29, 1797 (1968).
- ¹⁵E. Wiesendanger and G. Guntherodt, *Solid State Commun.* 14, 303 (1974).
- ¹⁶P. Pertosa, G. Hollinger, and F. M. Michel-Calendini, *Phys. Rev. B* 18, 5177 (1978).
- ¹⁷F. M. Michel-Calendini, H. Chermette, and J. Weber, *J. Phys. C* 13, 1427 (1980).
- ¹⁸L. F. Mattheiss, *Phys. Rev. B* 6, 4718 (1972).
- ¹⁹W. Cochran, *Adv. Phys.* 9, 387 (1960).
- ²⁰J. D. Axe, *Phys. Rev.* 157, 429 (1967).
- ²¹A. W. Hewatt, *J. Phys. C* 6, 1074 (1973).
- ²²R. A. Cowley, *Phys. Rev.* 134, A981 (1964).
- ²³J. Bouillot, Ph.D thesis (Dijon, 1977) (unpublished).
- ²⁴A. H. Kahn and A. J. Leyendeker, *Phys. Rev.* 135, A1321 (1964).
- ²⁵S. H. Wemple and M. Di Domenico, *Applied Solid State Science* (Academic, New York, 1972).
- ²⁶M. Di Domenico and S. H. Wemple, *J. Appl. Phys.* 40, 720 (1969).